https://doi.org/10.1007/s41230-026-5175-5

Dimensional control of turbine blades via RSM-based process parameter optimization in investment casting

Sheng-jie Ren[1, 2, 3], Rui-yuan Zhang[1, 2], Sheng Meng[2], Hang-yu Li[1], Wen-jing Wang[1], Zhong-min Xiao[3], and *Kun Bu[1, 2]

1. Key Laboratory of High Performance Manufacturing for Aero Engine, Ministry of Industry and Information Technology, Northwestern Polytechnical University, Xi'an 710072, China

2. Engineering Research Center of Advanced Manufacturing Technology for Aero Engine, Ministry of Education, Northwestern Polytechnical University, Xi'an 710072, China

3. School of Mechanical and Aerospace Engineering, Nanyang Technological University, Singapore 639798, Singapore

Abstract: To address the dimensional accuracy challenges in investment casting of DD6 nickel-based superalloy hollow turbine blades, a multi-parameter collaborative optimization and deformation response prediction method based on response surface methodology was proposed. Using a Box-Behnken design, with pouring temperature, shell temperature, and withdrawal rate as key variables, deformation response data were obtained through numerical simulation, and a second-order model incorporating linear, interaction, and quadratic terms was established to characterize the nonlinear coupling effects of process parameters on dimensional deformation. The results indicate that withdrawal rate is the dominant factor influencing deformation, while shell temperature exhibits a pronounced "U"-shaped nonlinear trend. Significant interactions between process parameters are also observed. The constructed model demonstrates high predictive accuracy, with R^2 of 0.978 and an RMSE of 0.0026 mm, and exhibits strong generalization capability, enabling the identification of optimal parameter combinations even beyond the simulated dataset. Compared with conventional orthogonal design methods, the maximum deformation of the optimized process was reduced from 0.2021 mm to 0.1905 mm, achieving an improvement of approximately 5.74%. This work provides a theoretical foundation and practical strategy for dimensional accuracy control and multi-parameter process optimization in the manufacturing of complex thin-walled castings.

Keywords: response surface method; turbine blade; process parameter optimization; investment casting

CLC numbers: TG146.1+5 **Document code:** A **Article ID:** 1672-6421(2026)03-451-11

1 Introduction

Investment casting is a critical manufacturing process for high-performance hollow turbine blades, in which process parameters exert a decisive influence on both the forming quality and dimensional accuracy of the castings[1, 2]. Blade dimensional accuracy is essential for reliable assembly and aerodynamic integrity, directly affecting energy-conversion efficiency and overall aeroengine performance[3]. With the increasing structural complexity and performance requirements of turbine blades, significant coupling effects have emerged among key process variables such as withdrawal rate, pouring temperature, and preheating temperature during casting[4, 5]. These interactions are recognized as major contributors to deformation and dimensional deviation in cast components[6-8]. Therefore, systematically identifying the dominant process parameters and their interactions has become a core challenge in improving the dimensional precision and consistency of turbine blades.

In recent years, extensive research has been conducted on solidification-based numerical analysis and process optimization in investment casting[4, 9-11]. These efforts have significantly contributed to shortening development cycles, reducing experimental costs, and improving product quality. Dini et al.[12] employed a single-factor control approach to investigate the effects of process parameters on residual stress and

***Kun Bu**

Female, Ph. D., Professor. Her research interests primarily focus on turbine blade investment casting and numerical simulation of its forming process.

E-mail: pukun89@nwpu.edu.cn

Received: 2025-07-27; Revised: 2025-09-10; Accepted: 2026-01-06

dimensional variation in castings. Ma et al.[13] studied the influence of temperature gradients and withdrawal rates on defect formation during Bridgman directional solidification. Miller et al.[14] determined optimal process conditions by analyzing the position and morphology of the solid-liquid interface, and found that a stabilized and planar interface is essential for reducing casting defects. Wang et al.[15] developed a two-dimensional response-surface model that elucidated the relationship between wax-injection parameters and dimensional accuracy, and reported that parameter interactions have a non-negligible effect on dimensional control. Galantucci et al.[16] used the finite element method to simulate temperature field evolution during directional solidification and examined the impact of filling temperature, withdrawal rate, and furnace geometry on the temperature distribution. For ring-on-ring castings, Wang et al.[17] established an RSM-based mapping between process variables and both casting diameter and ovality. Kavitha et al.[18] employed a Box-Behnken design (BBD) to study the effects of pouring temperature, insert temperature, insert thickness, and surface roughness on the bond strength of Al-SS bimetallic parts in lost-foam composite casting, achieving an optimized strength of 17.04 MPa. Tian et al.[19] conducted orthogonal experiments to optimize casting process parameters, resulting in a 21.8% reduction in flange deformation. Niranjan et al.[20] designed a multi-factor, multi-level experimental scheme and validated the derived model, achieving a prediction accuracy exceeding 95% for the mechanical properties of the material.

Although previous studies have made notable progress in process parameter optimization, most remain limited to single-factor analysis, making it difficult to fully capture the interactions among variables and their synergistic effects on dimensional deformation[21-23]. In contrast, response surface methodology (RSM) offers the ability to construct high-order regression models incorporating interaction terms, while maintaining strong modeling accuracy and optimization capability. These features make it suitable for addressing the complexity and coupling investment casting process optimization.

Based on the above analysis, RSM was employed to optimize multiple process parameters involved in turbine blade investment casting, with the experimental design based on the BBD. The dimensional deformation behavior of turbine blades under different process conditions was systematically investigated.

2 Materials and methods

2.1 Experimental procedure

The directional solidification of single-crystal turbine blades is a complex process involving the coupling of multiple physical fields and influencing factors. From alloy melting to solidification, the entire process is conducted under vacuum conditions.

As illustrated in Fig. 1, the directional solidification system and its corresponding numerical modeling process for single-crystal turbine blades are presented. Figure 1(a) shows the structural schematic of the casting, including the gating system, ceramic core, blade body, starter block, and grain selector, which together define the functional layout along the vertical axis. Figure 1(b) illustrates the numerical simulation model, incorporating the mold geometry and the heating-cooling zone configuration designed to reproduce the temperature gradient environment. Figure 1(c) displays the experimental directional solidification apparatus, in which the mold is gradually withdrawn from the heating furnace into the cooling chamber to achieve controlled unidirectional solidification. The entire process was carried out in a vacuum induction furnace, sequentially involving alloy melting, mold filling, directional solidification, and constraint removal.

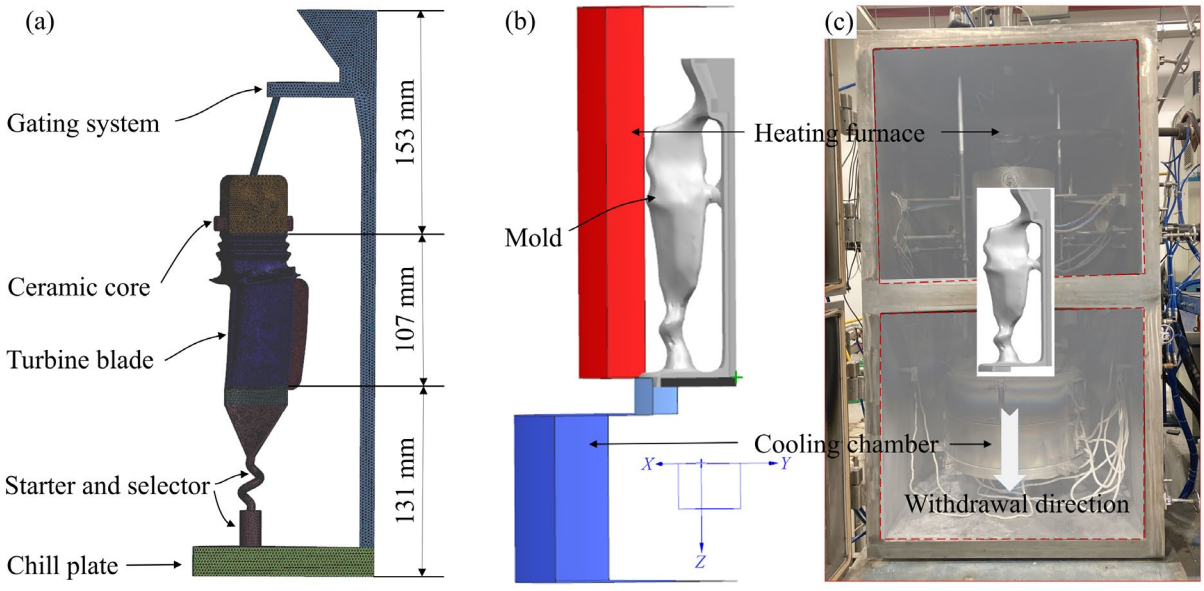

Fig. 1: Experimentation and modeling of turbine blade directional solidification: (a) assembly of the casting system including gating system, ceramic core, and grain selector; (b) numerical simulation model; (c) vacuum furnace

In the experiment, 5 kg of DD6 single-crystal superalloy was melted under a vacuum pressure of 3×10^{-3} Pa and subsequently poured from the top into the shell mold, which had a thickness of 7.5 mm. After a short holding period to achieve thermal equilibrium, the mold was withdrawn downward at a rate of 2.5 mm·min^{-1}, enabling its gradual transition from the high-temperature zone to the low-temperature zone. This movement established a longitudinal temperature gradient along the blade axis, promoting the formation of a directionally solidified structure. The composition of the DD6 superalloy used is shown in Table 1.

During the early stage of solidification, heat transfer occurred primarily via thermal conduction in the downward direction. However, as the solid-liquid interface progressed upward, the thermal conductivity decreased and the dominant heat dissipation mechanism gradually shifted from conduction to radiation[24-27].

To improve computational accuracy and efficiency, a non-uniform finite element mesh was employed in the model, with element sizes ranging from 0.5 to 15 mm, as shown in Fig. 2. Approximately 1.07 million elements were generated in total, with local mesh refinement applied to critical regions such as the blade root junction and interface transition zones. Specifically, the mesh size at the blade root was set to 1 mm, while the platform and trailing edge adopted 0.5 mm, with the transition region gradually varying between the two.

Table 1: Nominal chemical composition of DD6 single-crystal superalloy

Element	C	Cr	Co	W	Mo	Al	Nb	Ta	Re	Hf	Ni
wt.%	0.2	4.3	9	8	2	5.7	1.2	7.2	2	0.1	Bal.

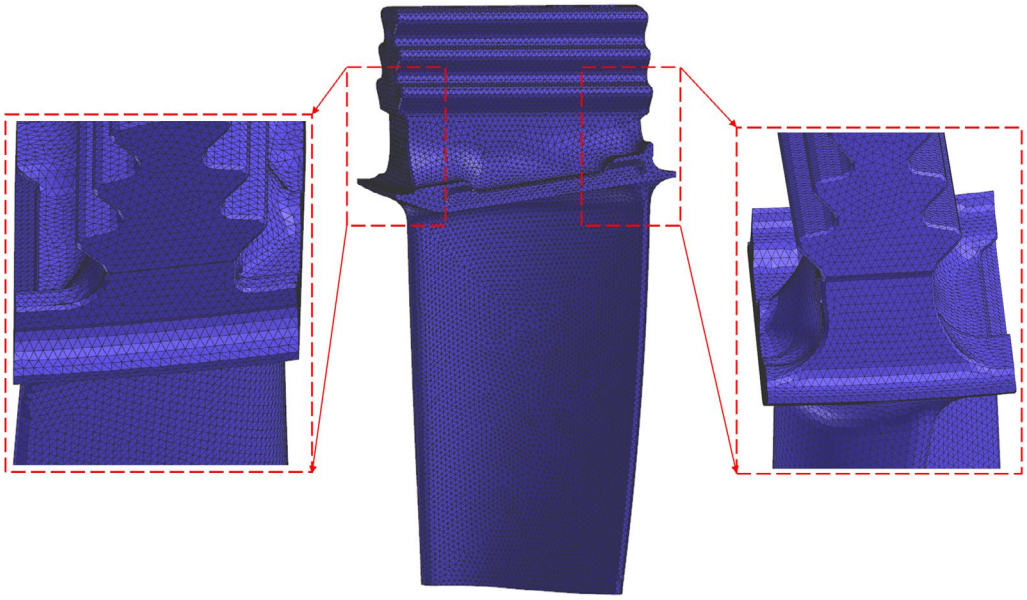

Fig. 2: Surface mesh of the gating system

2.2 Boundary conditions

To ensure the accuracy of the simulation, key thermophysical parameters of the DD6 nickel-based superalloy, such as thermal conductivity, density, enthalpy, and solid fraction, were calibrated based on experimental measurements and calculations using JMatPro and ProCAST. The results are shown in Fig. 3 and serve as essential input for the subsequent coupled thermo-mechanical simulations of the temperature and stress fields.

The heat transfer between the furnace and the shell mold was primarily considered to occur via thermal radiation, with the radiation direction oriented toward the interior of the furnace. The radiation emissivity was set to 0.7 according to Refs. [4, 28].

Under these assumptions the equation for heat transfer in castings can be simplified to[29, 30]:

$$\rho c\frac{\partial T}{\partial t}=\lambda\left(\frac{\partial^2 T}{\partial x^2}+\frac{\partial^2 T}{\partial y^2}+\frac{\partial^2 T}{\partial z^2}\right)+Q \tag{1}$$

where ρ is the density, kg·m^{-3}; c is the specific heat, J·(kg·K)$^{-1}$; T is temperature, K; x, y, and z represent coordinates; λ is the heat conductivity, W·(m·K)$^{-1}$; Q is the radiation heat between the casting surface and its environment, W·m^{-3}.

The temperature of the liquid metal is uniformly distributed at the initial time of solidification.

$$T\left(x,y,z,t\right)\big|_{t=0}=T_0 \tag{2}$$

where T_0 is the initial pouring temperature.

According to the Stefan-Boltzmann law, the radiation heat flux between the inner surface of the furnace and the outer surface of the shell mold is expressed as:

$$q=\varepsilon\sigma(T_s^4-T_a^4) \tag{3}$$

where q is the heat flux density, J·m^{-2}; ε is the emissivity, value

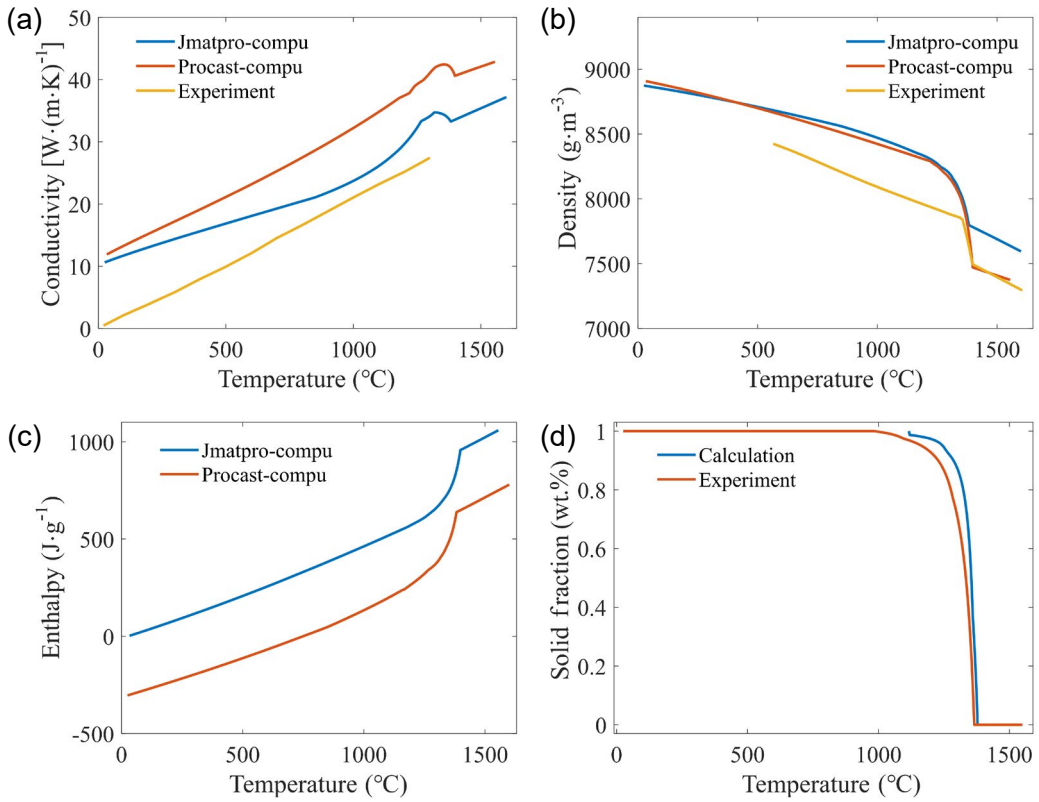

Fig. 3: Partial thermophysical parameters of nickel-based superalloy DD6: (a) conductivity; (b) density; (c) enthalpy; (d) solid fraction

in [0, 1]; σ is the Stefan-Boltzmann constant; T_s and T_a are surface and ambient temperature, respectively.

2.3 Response surface method

In this study, RSM was employed to establish the functional relationships between input variables and response variables. The response is typically fitted using a second-order polynomial regression model, which is expressed as follows[31-33]:

$$Y = \beta_0 + \sum_{i=1}^{k} \beta_i X_i + \sum_{i=1}^{k} \sum_{j=1}^{k} \beta_{ij} X_i X_j + \sum_{i=1}^{k} \beta_{ii} X_i^2 \qquad (4)$$

where Y represents the predicted response, X is the independent variables, and β corresponds to the regression coefficients.

The BBD is an efficient experimental design method that requires fewer runs than central composite designs while still estimating interaction and quadratic effects. In this study, BBD was integrated with RSM to investigate the influence of multiple factors and their interactions on the response variable. Figure 4 presents the geometric layout of experimental points constructed using the BBD, aimed at exploring the influence of three key process parameters on dimensional accuracy during the investment casting of turbine blades. As one of the most used experimental designs in RSM, BBD is particularly suitable for optimization involving two to five factors[34-37].

In the 3D parameter space in Fig. 4, blue solid spheres denote the BBD design points, positioned at the midpoints of the edges of the cubic design space, while the red central point represents the repeated center run used for estimating experimental error and model curvature. This structured

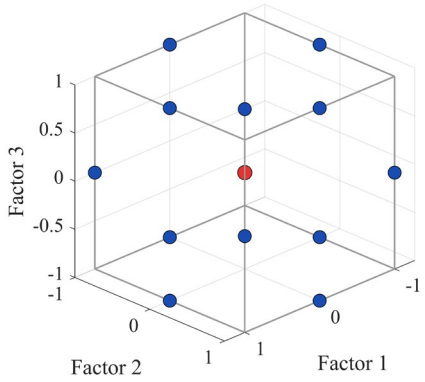

Fig. 4: Spatial distribution of BBD points in a three-factor parameter space for investment casting optimization

sampling strategy ensures balanced evaluation of parameter interactions while avoiding extreme corner points, thereby improving both the safety and statistical robustness of the experimental plan.

This design requires the specification of three levels for each factor: the high level (+1), the low level (−1), and the center point (0). Notably, all experiments are confined within the defined design space and do not involve extreme or extrapolated conditions beyond the specified range.

Pouring temperature T_p (°C), shell temperature T_s (°C), and withdrawal rate v (mm·min^{-1}) were selected as the process variables, while the blade deformation was taken as the target response. As shown in Table 2, each of the three process parameters was set at three levels, coded as −1, 0, and +1, corresponding to the low, center, and high levels,

respectively. The process parameter ranges were determined with reference to reported process windows for DD6 and related single-crystal superalloys[19], and further constrained by shop-floor requirements and furnace temperature-control capability.

The experimental scheme and the corresponding response values are presented in Table 3. Based on the three selected process parameters, a total of 17 experimental runs were generated. The resulting deformation responses ranged from 0.18 mm to 0.23 mm. A nonlinear mathematical model was subsequently developed based on the BBD framework to describe the response surface.

Table 2: Experimental variables and levels

Process parameters	Symbol	Levels		
		−1	0	1
Pouring temperature (°C)	A	1,520	1,550	1,580
Shell temperature (°C)	B	1,450	1,475	1,500
Withdrawal rate (mm·min^{-1})	C	2	2.5	3

Table 3: Some experimental matrices for RSM designs based on three level variables

No.	Influencing factors			Response deformation (mm)
	A	B	C	
1	1,520	1,450	2.5	0.2170
2	1,520	1,500	2.5	0.2204
3	1,520	1,475	2	0.2039
4	1,520	1,475	3	0.2232
5	1,550	1,450	2	0.2047
6	1,550	1,500	2	0.2043
7	1,550	1,450	3	0.2277
8	1,550	1,500	3	0.2261
9	1,550	1,475	2.5	0.2056
10	1,550	1,475	2.5	0.2057
11	1,550	1,475	2.5	0.2053
12	1,550	1,475	2.5	0.2052
13	1,550	1,475	2.5	0.2051
14	1,580	1,450	2.5	0.2103
15	1,580	1,500	2.5	0.2150
16	1,580	1,475	2	0.2021
17	1,580	1,475	3	0.2131

3 Results and discussion

3.1 Directional solidification physical field analysis

As shown in Fig. 5, temperature contour maps at t=0; 1,000 s; 3,000 s; 5,000 s; 7,000 s; and 9,000 s depict the evolution of the temperature field during investment casting under the baseline setting (coded level 0: T_p=1,550 °C, T_s=1,475 °C, v=2.5 mm·min^{-1}). The results reveal a distinct vertical temperature gradient, with nearly horizontal isothermal lines, indicating that heat flow is predominantly conducted along the axial direction. This thermal condition facilitates the preferential vertical growth of the single crystal, which is consistent with the theoretical principles of directional solidification for single-crystal blades.

Dimensional deviation is a critical issue in the investment casting of turbine blades. Minimizing deformation and ensuring high surface accuracy are essential objectives for improving casting quality. As illustrated in Fig. 6, the displacement contour maps at the initial moment, 1,000 s; 3,000 s; 5,000 s; 7,000 s; and 9,000 s display the evolution of the displacement field throughout the casting process. As the solidification process proceeds, noticeable deformation begins to appear in the casting after approximately 3,000 s. In the later stage, the deformation becomes more pronounced, with the maximum displacement concentrated at the trailing edge.

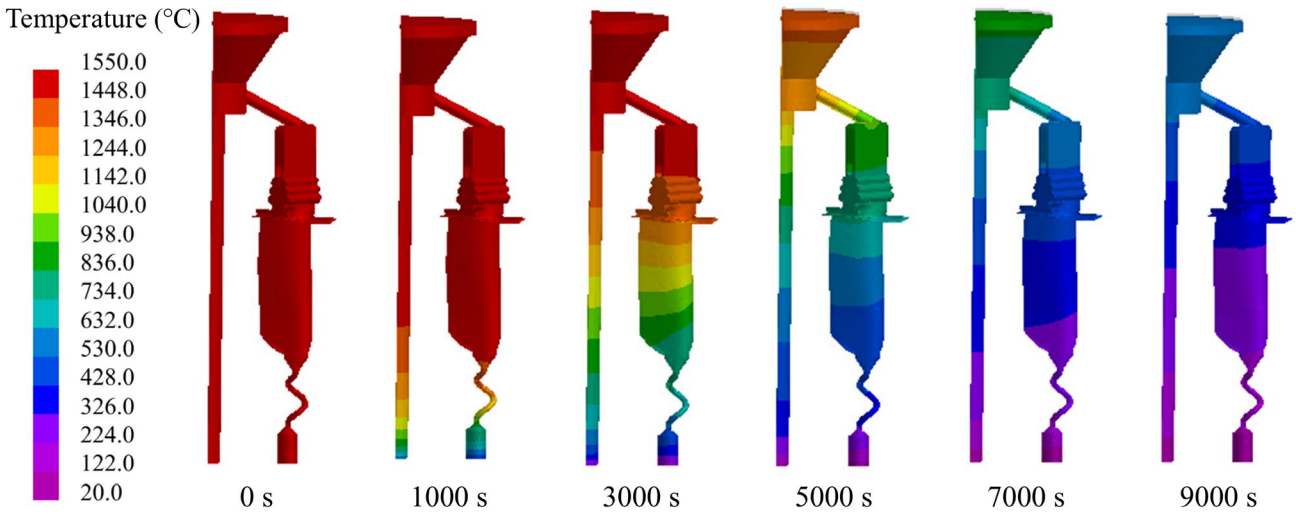

Fig. 5: Temperature field distribution during directional solidification of castings

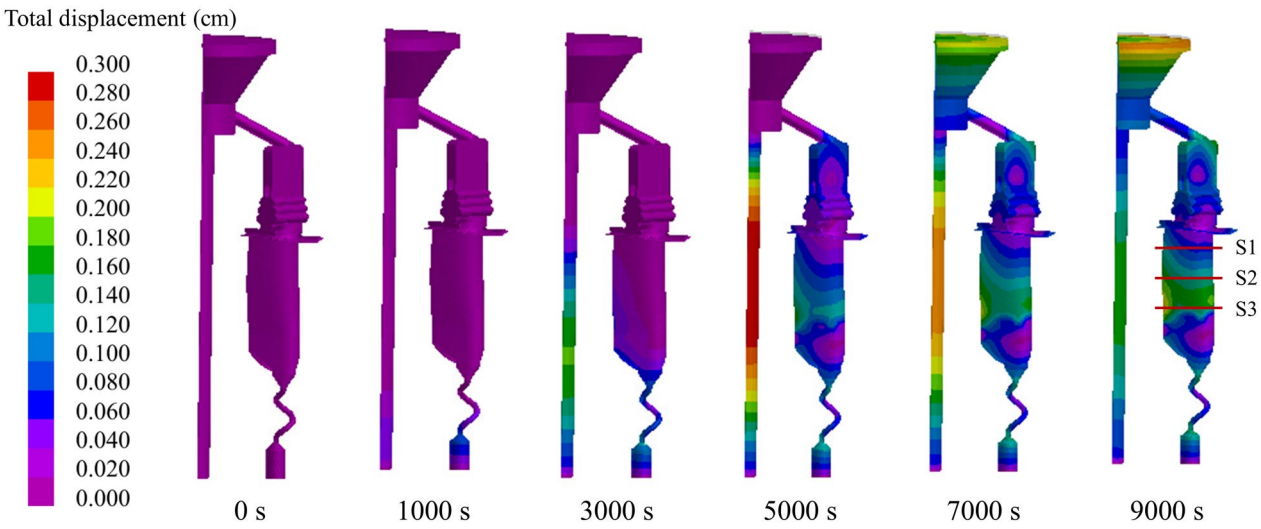

Fig. 6: Displacement field distribution during directional solidification of castings

These distributions enable a clear and intuitive observation of the deformation magnitude and trends in various regions of the casting, including the platform and trailing edge, thereby providing valuable insights into the overall deformation behavior during the entire investment casting process.

As shown in Figs. 7 and 8, the total displacement is mapped on three cross-sections at 20% (S1), 50% (S2), and 80% (S3) of the blade height (Fig. 6), with a common color scale for comparison. Figure 7 indicates that as the pouring temperature T_p increases from 1,520 to 1,580 °C, the displacement on all three sections decreases overall, most noticeably on S2. On each section, the trailing edge exhibits larger displacement than the leading edge, and across sections the magnitude follows S1<S2<S3; the maximum consistently occurs at the trailing edge of S3. Figure 8 shows that the shell preheating temperature T_s produces a U-shaped response, with the minimum displacement appearing near 1,475 °C.

Snapshots taken for panel at different time-step indices under different withdrawal rates are shown in Fig. 9. Figure 9(a) shows the mushy zone shape at time-step indices 3,000; 2,350; and 1,950 at a withdrawal rate of 2 mm·min^{-1}. Figure 9(b) shows the mushy zone shape at time-step indices 2,500; 1,950; and 1,600 at a withdrawal rate of 2.5 mm·min^{-1}. Figure 9(c) shows the mushy zone shape at time-step indices 2,100; 1,700; and 1,400 at a withdrawal rate of 3 mm·min^{-1}. The mushy zone at three withdrawal rates appears as an inclined band bounded by the liquidus (T_L) and solidus (T_S) isotherms and migrates upward with withdrawal rates. As the mushy zone moves upward with increasing withdrawal rates, the solid-liquid interface becomes straighter, which is particularly evident near

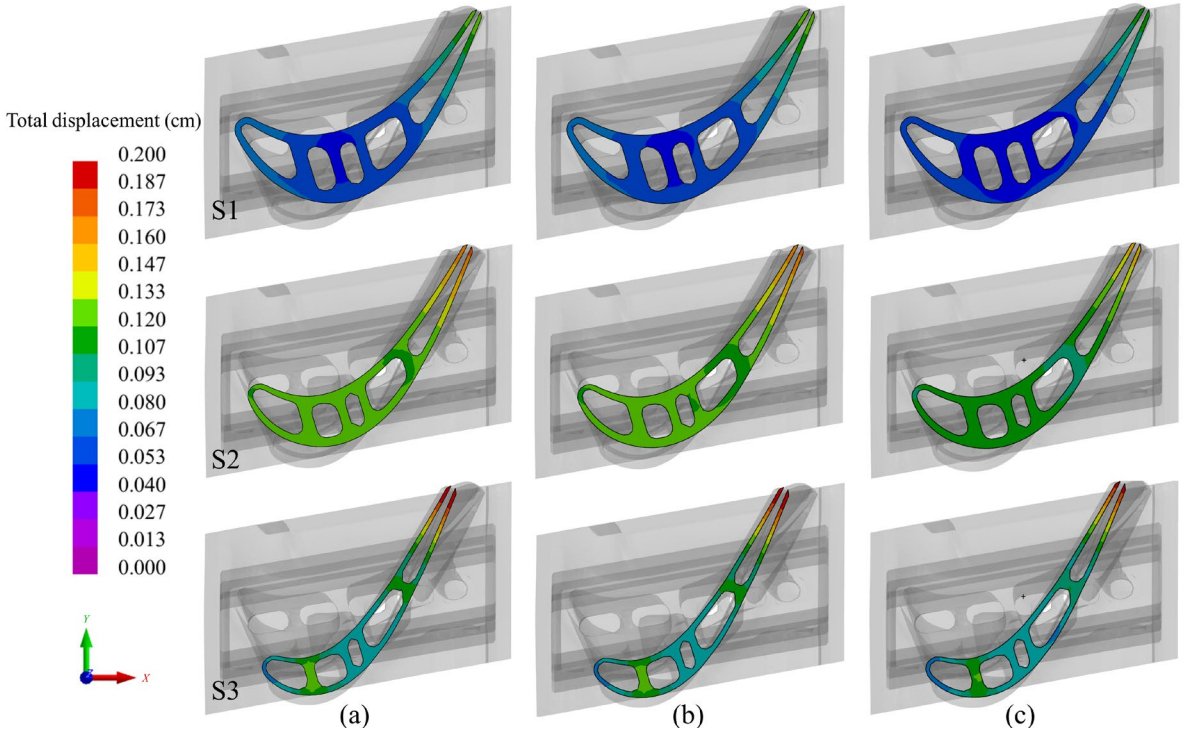

Fig. 7: Total displacement at different pouring temperatures: (a) 1,520 °C; (b) 1,550 °C; (c) 1,580 °C

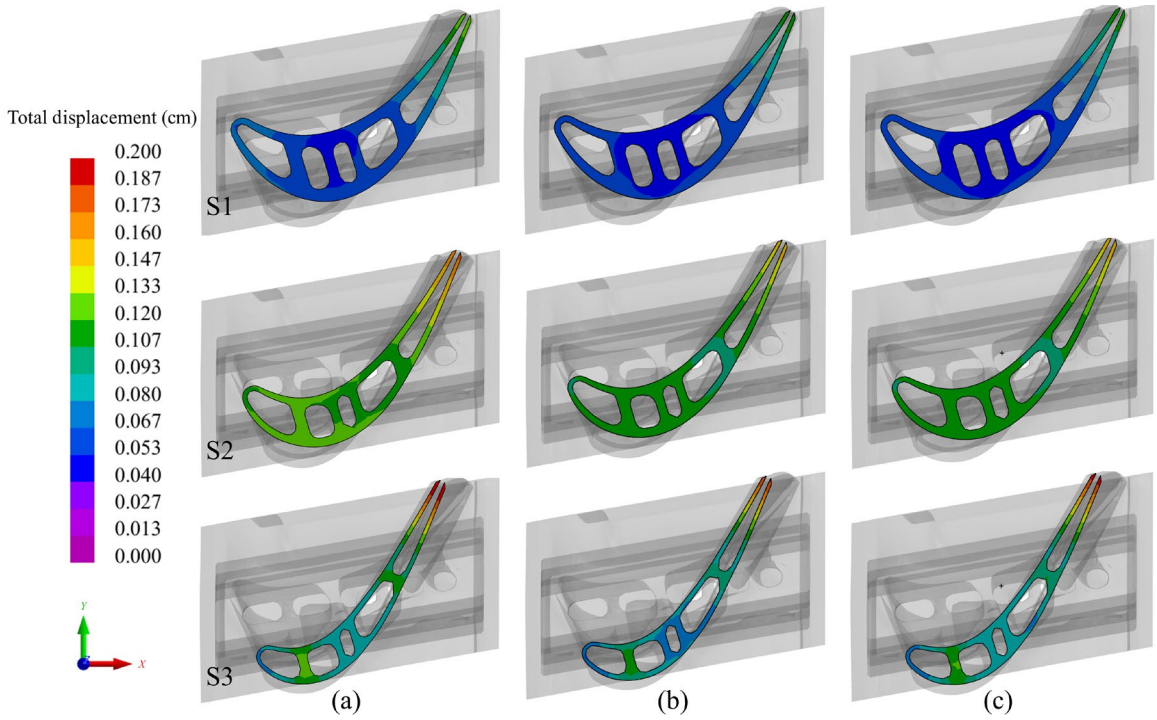

Fig. 8: Total displacement at different shell temperatures: (a) 1,450 °C; (b) 1,475 °C; (c) 1,500 °C

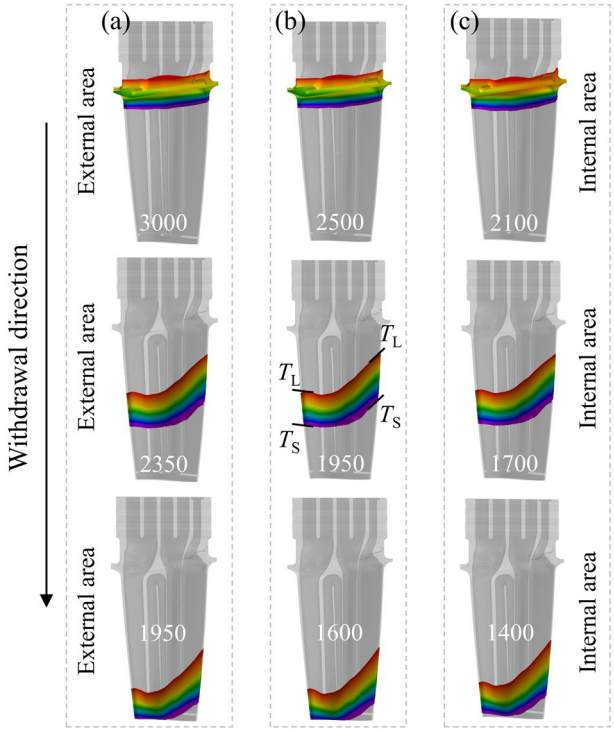

Fig. 9: Mushy zone shape along blade height for withdrawal rates of 2 mm·min^{-1} (a), 2.5 mm·min^{-1} (b), and 3 mm·min^{-1} (c). The arrow indicates the withdrawal direction

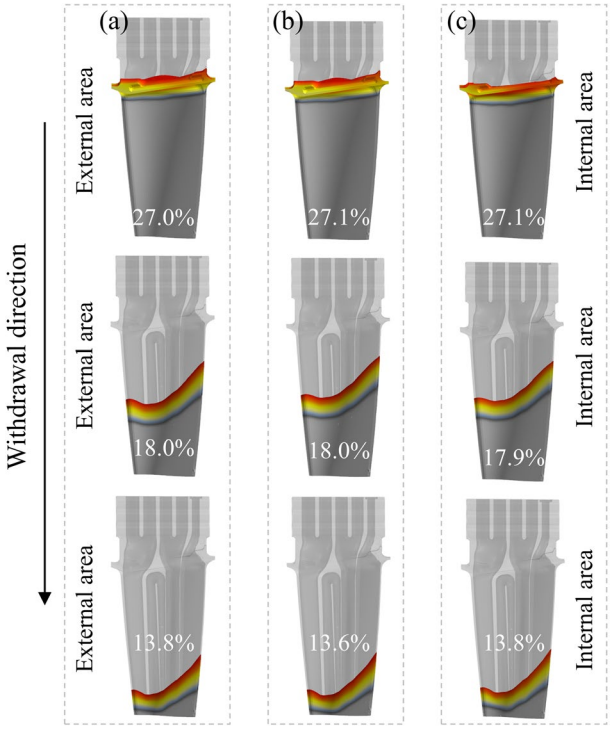

Fig. 10: Solid fraction along blade height for withdrawal rates of 2 mm·min^{-1} (a), 2.5 mm·min^{-1} (b), and 3 mm·min^{-1} (c). The arrow indicates the withdrawal direction

the edge plate region. Because the leading edge adjacent to the external side cools faster than the trailing edge region adjacent to the internal side, the mushy zone exhibits an asymmetric, upward-tilted morphology.

Solid fraction maps were extracted on three spanwise sections under withdrawal rates of 2, 2.5, and 3 mm·min^{-1}. As shown in Fig. 10, the fraction increases from about 13.6% to 27.1% as the casting moves downward. At the same height, the solid fraction values show slight differences, primarily because the results were extracted at fixed output intervals (i.e., discrete time steps) rather than due to a dominant effect of the parameters themselves. Overall, the spatial pattern of the solid fraction is consistent with the mushy zone distribution trend shown in Fig. 9.

3.2 Influence of a single process parameter on casting dimensions

To analyze the effect of each individual parameter while holding the other two at their center levels, response surface slice plots were generated. These plots illustrate how the target function–deformation magnitude varies with changes in a single parameter under controlled conditions. The results are presented in Fig. 11.

Casting deformation slightly decreases with increasing pouring temperature, indicating low sensitivity to this parameter. In contrast, shell temperatures show a pronounced nonlinear effect on deformation, with a near "U"-shaped response curve. This suggests the existence of an optimal temperature range, where both excessively high and low values may lead to increased deformation. Withdrawal rate is identified as the most influential factor, with deformation increasing significantly as the rate increases, implying that a lower withdrawal rate is preferable for minimizing dimensional deviation.

Furthermore, the distribution of the confidence intervals indicates that the model yields higher predictive accuracy near the center of the design space. However, increased uncertainty is observed at the boundaries, likely due to a lower density of experimental data in those regions.

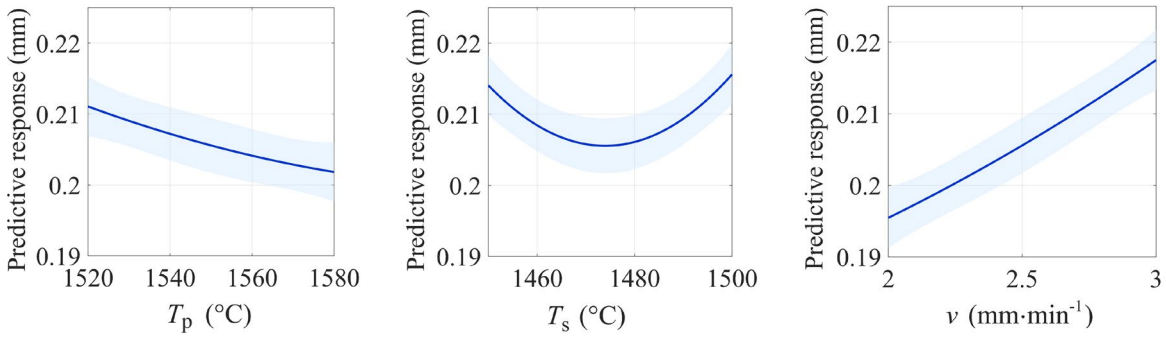

Fig. 11: Effect of three process parameters on predicted response

3.3 RSM-based process optimization results

The response values, representing the dimensional deviations of the castings under different process parameter combinations, were obtained through numerical simulation or experiments. These responses were modeled as functions of coded variables using a second-order response surface model incorporating linear, quadratic, and interaction terms. The resulting model was employed to characterize the individual effects of each process parameter on casting deformation, as well as the interactions among them.

$$\begin{aligned} Y = {} & 0.20557 - 0.00463\mathrm{A} + 0.00077\mathrm{B} + 0.01102\mathrm{C} \\ & + 0.00033\mathrm{AB} + 0.00117\mathrm{AC} - 0.00032\mathrm{BC} \\ & + 0.00088\mathrm{A}^2 + 0.00926\mathrm{B}^2 + 0.00091\mathrm{C}^2 \end{aligned} \quad (5)$$

In the model, A, B, and C denote the coded variables corresponding to the pouring temperature, shell temperature, and withdrawal rate, respectively, with each ranging from −1 to +1. The linear relationships between the actual physical parameters and the coded variables are detailed in Table 2. This model facilitates the analysis of main effects, interaction effects, and nonlinear behaviors of the process parameters, providing a theoretical foundation for subsequent optimization.

The root mean square error (RMSE) and the coefficient of determination (R^2) were used to evaluate the accuracy of the response surface model. The specific equation is as follows:

$$\mathrm{RMSE} = \sqrt{\frac{1}{n}\sum_{i=1}^{n}\left(y_i - \hat{y}_i\right)^2} \quad (6)$$

$$R^2 = 1 - \left(\frac{\sum_{i=1}^{n}\left(y_i - \hat{y}_i\right)^2}{\sum_{i=1}^{n}\left(\bar{y}_i - \hat{y}_i\right)^2}\right) \quad (7)$$

where y_i and $\hat{y}_i$ are the true value and predicted value of the casting samples, respectively, and $\bar{y}_i$ denotes the sample mean. The smaller the RMSE value, the closer the R^2 is to 1, i.e., the smaller the difference between the model's predicted value and the true value, the better the model's performance.

Analysis of variance (ANOVA) was used to quantify the percentage contributions of the process parameters to the target responses, thereby revealing the relative significance of each controlled factor. ANOVA for blade deformation is summarized in Table 4. The reduced quadratic model shows strong goodness of fit (R^2=0.978; RMSE=0.0026 mm) and is significant overall (F=42.85, p<0.0001). Among the terms, the withdrawal rate (C) is dominant, and pouring temperature (A) is also significant (F=37.35, p=0.0005), whereas the linear effect of shell temperature (B) is not obvious. By contrast, the quadratic term B^2 is highly significant, indicating a pronounced U-shaped dependence on T_s.

As shown in Fig. 12, 3D response surfaces and 2D contour plots were generated based on the RSM model to illustrate the interaction effects of process parameters on flange deformation. In each case, the third parameter was fixed at its central level.

Figures 12(a) and (b) show a curved response surface, indicating strong interaction between T_s and T_p. At a low T_p value, the deformation is more sensitive to T_s; at a high T_p value, the surface flattens, suggesting greater stability. The

Table 4: ANOVA for the reduced quadratic RSM model of casting deformation

Variable	Statistical analysis				
	Sum of squares	df	Mean square	*F*-value	*P*-value
Model	0.0014	9	6.760E-06	42.85	<0.0001
A-pouring temperature	0.0001	1	0.0001	37.35	0.0005
B-shell temperature	4.285E-06	1	4.285E-06	1.20	0.3100
C-withdrawal rate	0.0009	1	0.0009	245.06	<0.0001
AB	6.281E-07	1	6.281E-07	0.1756	0.6878
AC	1.626E-08	1	1.626E-08	0.0045	0.9481
BC	3.994E-07	1	3.994E-07	0.1116	0.7481
A^2	0.0000	1	0.0000	2.81	0.1378
B^2	0.0003	1	0.0003	91.51	<0.0001
C^2	9.516E-06	1	9.516E-06	2.66	0.1469
Residual	0.0000	7	3.578E-06		
Lack of fit	0.0000	3	8.231E-06	93.66	0.0004
Cor total	0.0014	16			

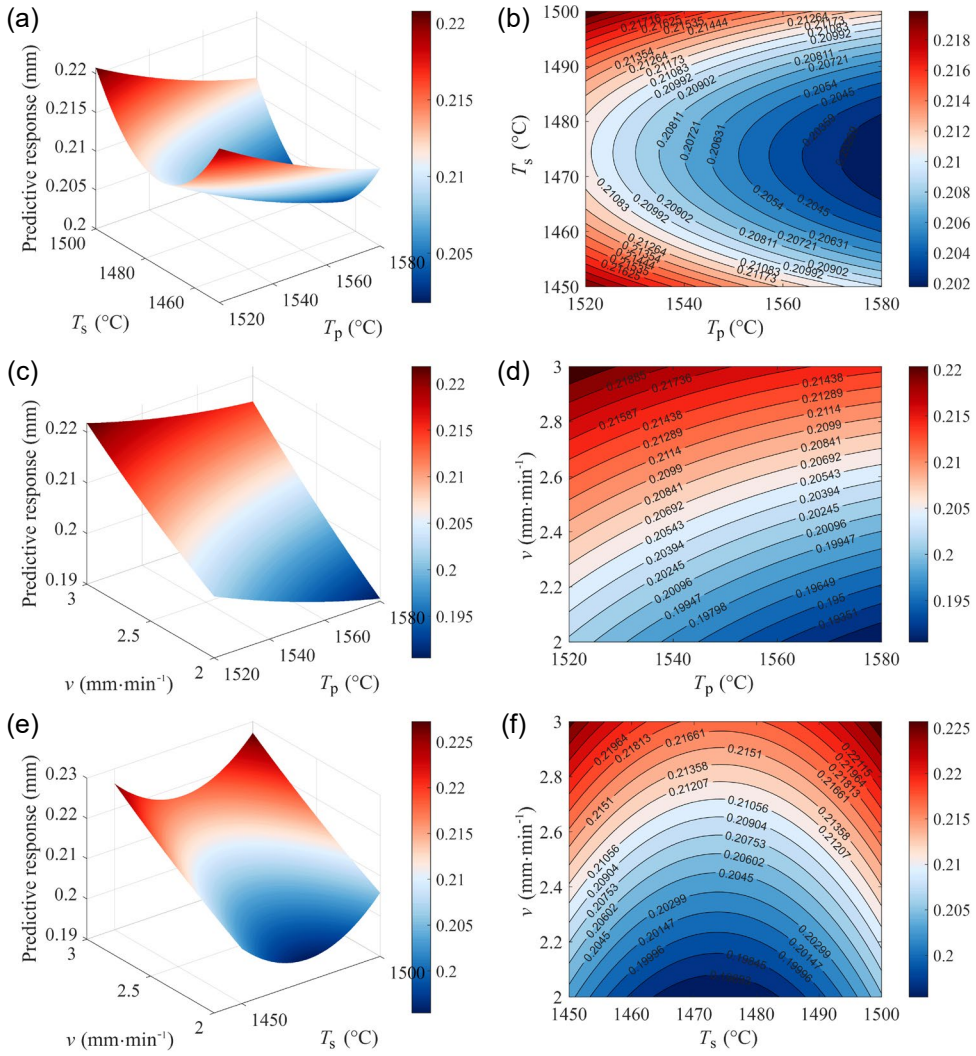

Fig. 12: Interaction effects of process parameters on deformation response of turbine blades: (a) pouring temperature vs. shell temperature; (c) pouring temperature vs. withdrawal rate; (e) shell temperature vs. withdrawal rate. (a), (c), and (e) are 3D response surface plots, and (b), (d), and (f) are the corresponding 2D contour plots for (a), (c), and (e), respectively

contour plot reveals an elliptical optimal region, with lower deformation in the medium-to-high temperature range.

Figures 12(c) and (d) show that deformation increases monotonically with v, confirming it as a dominant factor. However, a higher T_p mitigates this trend. Dense contour lines at high v indicate steep response gradients and highlight the need to tightly control v for dimensional accuracy.

Figures 12(e) and (f) show a distinct valley shape, indicating an optimal withdrawal rate range within a certain T_s interval. Deformation decreases as T_s drops, but rises again at low T_s, likely due to reduced shell stiffness and increased thermal stress. Symmetric contour lines further confirm the existence of an optimal region.

Based on the established model, an objective function was defined to minimize the response value. Constrained optimization was performed within the coded variable range of [−1, 1] to identify the optimal parameter combination corresponding to the minimum deformation. The optimal solution was then mapped back to actual physical values using linear interpolation, as summarized in Table 5.

As shown in Table 5, the optimal parameters obtained by RSM, namely a pouring temperature of 1,580 °C, a shell temperature of 1,473 °C, and a withdrawal rate of 2 mm·min^{-1}, effectively reduce the deformation from 0.2021 mm to 0.1905 mm, corresponding to a reduction of approximately 5.74%.

The red point in Fig. 13 represents the optimized parameter combination obtained via response surface modeling. Unlike orthogonal experimental designs limited to discrete factor levels, RSM builds a continuous regression model across the design space, enabling the identification of optimal conditions beyond the original design points.

Notably, the optimal solution lies within the interior of the design cube but does not coincide with any simulated experiment, highlighting the model's strong interpolation and generalization capabilities. In comparison with Ref. [15], which applied RSM to predict the average diameter and ovality of ring-to-ring castings with relatively simple geometries, the present study focuses on a complex hollow turbine blade and establishes a quantitative mapping between process parameters and blade deformation. This comparison demonstrates that RSM is not only effective for simple casting geometries, but also capable of capturing nonlinear, multi-factor interactions in more complex investment casting components, thereby enabling the identification of improved solutions in previously unexplored regions.

Table 5: Comparison of optimization results between orthogonal and RSM for dimensional deviation minimization of turbine blades

Method	T_p	T_s	v	Response (mm)
Orthogonal	1,580	1,475	2	0.2021
RSM	1,580	1,473	2	0.1905

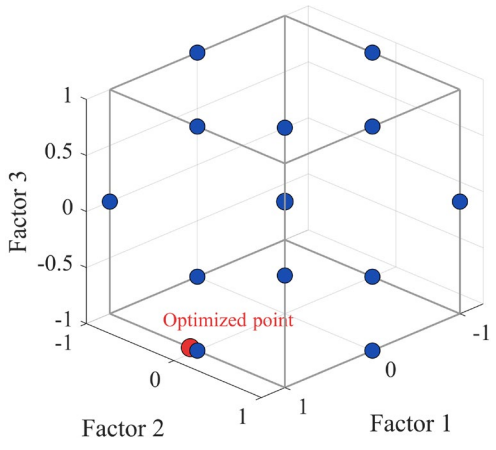

Fig. 13: Location of the optimized solution in normalized BBD space

4 Conclusions

Based on RSM, a predictive model for dimensional deformation and process parameter optimization was developed for the investment casting of turbine blades. The effects of key parameters, including pouring temperature, shell temperature, and withdrawal rate, on the dimensional response were systematically investigated. The main conclusions are as follows:

(1) Sensitivity analysis reveals that withdrawal rate is the dominant factor, while shell temperature exhibits a "U"-shaped nonlinear relationship with deformation. Significant interactions among parameters are observed, indicating the need for coordinated regulation to optimize forming quality.

(2) The constructed second-order RSM model demonstrates strong fitting accuracy, with a coefficient of determination R^2=0.978 and a RMSE of 0.0026 mm. The model effectively captures the complex nonlinear relationships between process parameters and deformation response.

(3) RSM enables the prediction of optimal parameter combinations beyond the originally tested design points. The optimized deformation is reduced from 0.2021 mm to 0.1905 mm, achieving a reduction of approximately 5.74%, thereby validating the adaptability and effectiveness of RSM in complex casting process optimization.

Acknowledgments

The authors greatly acknowledge the financial support from the National Science and Technology Major Project (No. J2019-VII-0013-0153) and the Innovation Capability Support Program of Shaanxi (No. 2022TD-60).

Conflict of interest

The authors declare that they have no known competing financial interests or personal relationships that could have appeared to influence the work reported in this paper.

References

[1] Reed R C. The superalloys fundamentals and applications. Cambridge: Cambridge University Press, 2008.
[2] Mathur H N, Panwisawas C, Jones C N, et al. Nucleation of recrystallisation in castings of single crystal Ni-based superalloys. Acta Materialia, 2017, 129: 112–123.
[3] Pollock T M. Alloy design for aircraft engines. Nature Materials, 2016, 15: 809–815.
[4] Ren S, Bu K, Zhang R, et al. Effect of constraint removal on single-crystal blade dimensions during investment casting. Journal of Manufacturing Processes, 2024, 119: 73–86.
[5] Kermanpur A, Mehrara M, Varahram N, et al. Improvement of grain structure and mechanical properties of a land based gas turbine blade directionally solidified with liquid metal cooling process. Materials Science and Technology, 2008, 24: 100–106.
[6] Xu Q, Zhang H, and Liu B. Multiscale modelling and simulation of single crystal superalloy turbine blade casting during directional solidification process. China Foundry, 2014, 11(4): 9–11.
[7] Singh R and Singh J. Investigating the effect of shape factor, slurry layers and pouring temperature in precision investment casting. Materials Science Forum, 2013, 751: 35–44.
[8] Ren S, Bu K, Mou S, et al. Control of dimensional accuracy of hollow turbine blades during investment casting. Journal of Manufacturing Processes, 2023, 99: 548–562.
[9] Qian C, Kaminer I, Chen H. A guidance to intelligent metamaterials and metamaterials intelligence. Nature Communications, 2025, 16: 1154.
[10] Pattnaik S, Karunakar D B, Jha P K. Developments in investment casting process–A review. Journal of Materials Processing Technology, 2012, 212: 2332–2348.
[11] Wang F, Liu Y, Yang Q, et al. Microscale stray grains formation in single-crystal turbine blades of Ni-based superalloys. Journal of Materials Science & Technology, 2024, 191: 134–145.
[12] Dini H, Andersson N E, Jarfors A E W. Effect of process parameters on distortion and residual stress of high-pressure die-cast AZ91D components. International Journal of Metalcasting, 2018, 12: 487–497.
[13] Ma D. Development of single crystal solidification technology for production of superalloy turbine blades. Acta Metallurgica Sinica, 2015, 51: 1179–1190. (In Chinese)
[14] Miller J D, Pollock T M. Process simulation for the directional solidification of a tri-crystal ring segment via the Bridgman and liquid-metal-cooling processes. Metallurgical and Materials Transactions: A, 2012, 43: 2414–2425.
[15] Wang D H, Sun F, Shu D, et al. Data-driven design of cast nickel-based superalloy and precision forming of complex castings. Acta Metallurgica Sinica, 2022, 58: 89–102. (In Chinese)
[16] Galantucci L M, Tricarico L. A computer-aided approach for the simulation of the directional-solidification process for gas turbine blades. Journal of Materials Processing Technology, 1998, 77: 160–165.
[17] Wang D, Yu J, Yang C, et al. Dimensional control of ring-to-ring casting with a data-driven approach during investment casting. The International Journal of Advanced Manufacturing Technology, 2022, 119: 691–704.
[18] Kavitha M, Raja V. Optimization of insert roughness and pouring conditions to maximize bond strength of (Cp)Al-SS304 bimetallic castings using RSM-GA coupled technique. Materials Today Communications, 2024, 39: 108754.
[19] Tian J W, Bu K, Song J H, et al. Optimization of investment casting process parameters to reduce warpage of turbine blade platform in DD6 alloy. China Foundry, 2017, 14(6): 469–477.
[20] Niranjan K, Lakshminarayanan P R. Optimization of process parameters for in situ casting of Al/TiB_2 composites through response surface methodology. Transactions of Nonferrous Metals Society of China, 2013, 23: 1269–1274.
[21] Szeliga D, Kubiak K, Sieniawski J. Control of liquidus isotherm shape during solidification of Ni-based superalloy of single crystal platforms. Journal of Materials Processing Technology, 2016, 234: 18–26.
[22] Ma D, Bührig-Polaczek A. Application of a heat conductor technique in the production of single-crystal turbine blades. Metallurgical and Materials Transactions: A, 2009, 40: 738–748.
[23] Aguilar J, Schievenbusch A, Kättlitz O. Investment casting technology for production of TiAl low pressure turbine blades–process engineering and parameter analysis. Intermetallics, 2011, 19: 757–761.
[24] Campbell J. Complete casting handbook, 2nd ed. Boston: Butterworth-Heinemann, 2015.
[25] Zhang H, Liu X, Ma D, et al. Digital twin for directional solidification of a single-crystal turbine blade. Acta Materialia, 2023, 244: 118579.
[26] Szeliga D, Kubiak K, Motyka M, et al. Directional solidification of Ni-based superalloy castings thermal analysis. Vacuum, 2016, 131: 327–342.
[27] Gromada M, Świeca A, Kostecki M, et al. Ceramic cores for turbine blades via injection moulding. Journal of Materials Processing Technology, 2015, 220: 107–112.
[28] Hallensleben P, Schaar H, Thome P, et al. On the evolution of cast microstructures during processing of single crystal Ni-base superalloys using a Bridgman seed technique. Materials & Design, 2017, 128: 98–111.
[29] Khandelwal H, Ravi B. Effect of varying part geometry and mold constraints on dimensional deviations of sand cast parts. International Journal on Interactive Design and Manufacturing (IJIDeM), 2025, 19: 4973–4986.
[30] Szeliga D. Effect of processing parameters and shape of blade on the solidification of single-crystal CMSX-4 Ni-based superalloy. Metallurgical and Materials Transactions: B, 2018, 49: 2550–2570.
[31] Allaix D L, Carbone V I. An improvement of the response surface method. Structural Safety, 2011, 33: 165–172.
[32] Kumar A, Ramadas H, Kumar C S, et al. Laser polishing of additive manufactured stainless-steel parts by line focused beam: A response surface method for improving surface finish. Journal of Manufacturing Processes, 2025, 133: 1310–1328.
[33] Jadhav P, Krishnan S, Patil R, et al. Improving biogas production with application of trimetallic nanoparticle using response surface methods. Renewable Energy, 2024, 234: 121199.
[34] Tiwari S, Kumar A, Gupta N, et al. Hydrogen storage systems performance and design parameters using response surface methods and sensitivity analysis. Renewable and Sustainable Energy Reviews, 2024, 202: 114628.
[35] Lal B, Dey A. Fretting wear characteristics of Ti6Al4V/TiC nano composites using response surface method. Tribology International, 2024, 193: 109412.
[36] Zheng P, Zhang H, Zhang Z, et al. Parameter optimization method of contra-rotating vertical axis wind turbine: Based on numerical simulation and response surface. Journal of Cleaner Production, 2024, 435: 140475.
[37] Rojas-López A G, Villarreal-Cervantes M G, Rodríguez-Molina A. Surrogate indirect adaptive controller tuning based on polynomial response surface method and bioinspired optimization: Application to the brushless direct current motor controller. Expert Systems with Applications, 2024, 245: 123070.